12-31-1987

State-Selective Studies of T→R, V Energy Transfer: The H+CO System

G. K. Chawla
Cornell University

George C. McBane
Grand Valley State University, mcbaneg@gvsu.edu

P. L. Houston
Cornell University

G. C. Schatz
Northwestern University

State-selective studies of T→R, V energy transfer: The H+CO system

G. K. Chawla, G. C. McBane, and P. L. Houston
Department of Chemistry, Cornell University, Ithaca, New York 14853-1301

G. C. Schatz
Department of Chemistry, Northwestern University, Evanston, Illinois 60201

(Received 27 November 1987; accepted 31 December 1987)

Collisional energy transfer from H atoms to CO($v=0, J\simeq 2$) has been studied at a collision energy of 1.58 ± 0.07 eV by photolyzing H_2S at 222 nm in a nozzle expansion with CO and probing the CO(v'', J'') levels using tunable VUV laser-induced fluorescence. The ratio CO($v''=1$)/CO($v''=0$) is found to be 0.1 ± 0.008. The rotational distribution of CO($v''=0$) peaks at $J'' \leqslant 11$ and decays gradually; population is still observed at $J'' \geqslant 45$. The rotational distribution of CO($v''=1$) is broad and peaks near $J''=20$. The experimental results are compared to quasiclassical trajectory calculations performed both on the H + CO surface of Bowman, Bittman, and Harding (BBH) and on the surface of Murrell and Rodriguez (MR). The experimental rotational distributions, particularly those for CO($v''=1$), show that the BBH surface is a better model than the MR surface. The most significant difference between the two surfaces appears to be that for energetically accessible regions of configuration space the derivative of the potential with respect to the CO distance is appreciable only in the HCO valley for the BBH surface, but is large for all H atom approaches in the MR potential. Because the H–CO geometry is bent in this valley, vibrational excitation on the BBH surface is accompanied by appreciable rotational excitation, as observed experimentally.

I. INTRODUCTION

Studies concerning the rotational–vibrational excitations of small molecules by collisions with translationally hot hydrogen atoms ($E_{\text{trans}} = 1$–3 eV) have received considerable attention in the past five years. Recent experimental progress in this area is due primarily to the technique of pulsed laser photolysis of diatomic or triatomic hydrides, a method which allows the production of fast, nearly monoenergetic hydrogen atoms.[1] Photolysis pulse widths of typically a few nanoseconds provide a temporally narrow source of H atoms and make possible the real-time detection of the collisionally excited product. A number of transient detection schemes have been employed to date, including the methods of infrared fluorescence detection,[2–9] infrared absorption of diode laser radiation,[10–14] coherent anti-Stokes Raman scattering,[15] and laser induced fluorescence.[16] The wide variety of collision systems studied further serves to illustrate the versatility of this technique. An excellent review is given by Flynn and Weston.[1]

One important aspect of such state-resolved energy transfer experiments is the opportunity to determine how the product rotational and vibrational state distributions reflect particular features of the intermolecular potential. Substantial progress has been made in the case of HCO, for which a very accurate *ab initio* surface has been generated by Bowman, Bittman, and Harding (BBH).[17] Various low-energy features of this surface, including the HCO potential well, have been verified by experiment. For example, kinetic measurements on the dissociation of HCO have provided estimates of the barrier to its formation from H + CO;[18] photoelectron spectroscopy of HCO^- has provided vibrational constants of HCO;[19] and photodissociation experiments on formaldehyde have provided estimates of the HCO well depth.[20] The experiments described in the present paper, conducted at 1.58 eV collision energy, address high-energy features of the HCO surface, which include the COH potential well and the isomerization barrier between the HCO and COH complexes.

Many previous studies are relevant to this high energy regime.[6–8,21–26] Wood, Flynn, and Weston used time-resolved infrared fluorescence in conjunction with a circular variable interference filter to demonstrate that CO produced following collision with 2.3 eV H atoms was rotationally excited to $12 < J < 20$ in addition to being vibrationally excited.[6] Wight and Leone subsequently examined the vibrational distribution in detail, again by using infrared fluorescence, and found that the CO($v''=1$–6) population distribution for collision with H atoms at 2.3 eV was 0.74, 0.15, 0.08, 0.01, 0.02, 0.01. The CO vibrational excitation was found to increase by more than a factor of 3 as the initial H atom energy was increased from 1.0 to 3.2 eV.[7,8] However, although Wight and Leone also observed that the rotational excitation was substantial, no specific information on the rotational distribution was obtained, nor was any information available concerning CO($v''=0, J''$). Geiger and Schatz[21] and Geiger, Schatz, and Harding[22] compared the results of classical trajectory calculations performed on potential surfaces obtained by fitting the Dunning surface[23] with a variant of the Sorbie–Murrell method[24] or by using a much improved surface based on calculations by Bowman, Bittman, and Harding.[17] Generally good agreement with the vibrational distribution at 2.3 eV was obtained, although the calculations for $v \geqslant 2$ were in better agreement with the ex-

 0021-9606/88/095481-08$02.10

perimental distribution than those for $v = 1$. An analysis of the trajectories indicated that the vibrationally excited CO molecules are produced in collisions of H primarily with the carbon end of CO, and that most of these collisions involve direct scattering of H with the inner repulsive wall of the HCO well. Two groups[25–27] have also studied resonances on the BBH surface which are caused by the HCO and COH well regions. It does not appear, however, that these resonances play a significant role in determining the vibrational distributions at the energies that have been studied so far. Recently, Murrell and Rodriguez (MR)[28] have developed a potential surface for H + CO based on a many-body expansion which reproduces the geometries and energies of the BBH surface near the minima and saddle points. The vibrational distributions obtained from this surface are also in reasonable agreement with experiment. However, one complication in all these comparisons between theory and experiment has been the uncertainty caused by possible multiple collisions in the experimental data.

In this paper we report the state-to-state, collisional energy transfer results of the H + CO system at 1.58 eV collision energy. A coexpansion of the H atom precursor (here H_2S) and CO in a free-jet expansion serves to define the precollision state by first, cooling the internal degrees of freedom of CO and second, narrowing the thermal spread of relative collision velocities between the H-atom precursor and CO. A rotationally resolved final state distribution of the collisionally excited CO is achieved by recording the CO laser-induced fluorescence spectrum, excited by a coherent and tunable vacuum ultraviolet (VUV) source. These techniques allow us to obtain fully resolved product state distributions, even for the vibrationally elastic but rotationally inelastic collisions that lead to the scattered CO($v'' = 0$) product.

The results of the present work include rotational state distributions for the $v'' = 0$ and $v'' = 1$ levels of CO scattered under single-collision conditions as well as quasiclassical trajectory (QCT) calculations performed on the BBH and MR surfaces. A reasonable correlation is found between features in the CO vibrational–rotational distribution and local region of closest H···CO approach on the HCO potential surface. QCT calculations on the BBH surface are in excellent agreement with observations. However, the MR surface is found to grossly overestimate the low J'', $v'' = 1$ collision cross section. The origin of this error involves an inappropriate description of the gradient of the H···CO potential with respect to the CO internuclear separation.

II. EXPERIMENTAL

The experimental technique involves the photolytic production of translationally hot H atoms and the VUV laser-induced fluorescence (LIF) detection of CO molecules which have undergone single-collision excitation by a hydrogen atom. H_2S is the hydrogen atom precursor chosen for this work.

Previous photodissociation studies[29] have shown H_2S to undergo prompt dissociation and to produce $\geqslant 82\%$ of the hydrogen atoms with a laboratory kinetic energy (for 222 nm photolysis) of 1.64 ± 0.07 eV. A premixed sample of 6% H_2S in purified CO is expanded through a pulsed valve[30] operating with 2 atm stagnation pressure. These expansion conditions cool CO to a measured rotational temperature of $\simeq 30$ K, for which the most probable CO rotational level is $J_{mp} = 2$. The H_2S photolysis light is supplied by a Nd:YAG-pumped dye laser system equipped with wavelength extending harmonic and sum-frequency generation crystals (Quanta-Ray DCR-2A, PDL-1, WEX-1). The 222 nm pulsed output of typically 3–4 mJ in 7 ns is loosely focused such that the spot size is 4 mm at the intersection zone of the photolysis beam and the H_2S + CO free jet. With the intersection zone situated $\simeq 15$ mm from the nozzle orifice (0.5 mm diameter), the calculated mean time between H + CO hard-sphere collisions is $\simeq 100$ ns. Calculations performed with an H_2S absorption cross section[31] of 1×10^{-18} cm^2 show that roughly 10^{12} H atoms are generated per photolysis laser pulse.

Following a nominally single-collision event between H and CO, the CO vibrational and rotational state distribution is measured by recording the VUV fluorescence excitation spectrum of the $A\,^1\Pi \leftarrow X\,^1\Sigma^+$ transition. Coherent VUV radiation in the wavelength region near 150 nm is generated by four-wave sum frequency mixing in magnesium vapor. This technique has been extensively described in earlier publications;[32–35] it produces broadly tunable VUV output with temporal and spectral widths of < 15 ns and 0.6 cm^{-1} (FWHM), respectively. With a VUV photon flux of 10^{12}/pulse, LIF detection of CO has been shown to have a sensitivity of 10^8 molecules/cm^3 per quantum state. The collimated VUV probe beam ($\simeq 1$ mm diameter), the photolysis beam, and the H_2S + CO free jet propagate in mutually orthogonal directions, while the VUV laser-induced fluorescence from CO is imaged in a direction at 45° to the VUV and photolysis beams by an $f/2$ optical system onto a solar-blind photomultiplier (PMT, EMR 541G-09-17). The PMT signal is amplified by a factor of 10 (LeCroy VV100B) and recorded by an integrator with 30 ns gate width (SRS Model SR-250) which is coupled to a computerized data acquisition system (DEC LSI 11/23). Using electronic systems similar to that for the CO fluorescence detection, the photolysis and VUV laser intensities are also recorded and used to normalize the CO LIF signals. A photolysis–VUV probe time delay of 200 ns is used in all experiments described. Since this time is sufficiently long for approximately two collisions of the fast H atoms, the effective H atom kinetic energy distribution is broader than the initial distribution by a few percent. However, the nascent character of the scattered CO distribution in these experiments is not affected on this time scale; very few CO molecules undergo more than one collision.

Background CO, present in the free-jet expansion, can contribute up to 25%–30% of the main collisionally excited CO population in the $v'' = 0$, $J'' > 11$ levels. (The $v'' = 0$, $J'' \leqslant 11$ levels are too heavily populated by background CO to make meaningful extractions of the collisionally induced population.) Real-time corrections for the CO background are made by using the active base line subtraction feature of the boxcar integrator. In this method the photolysis laser is

fired only on every other VUV probe pulse, and the averaging circuitry takes the difference between the main (collisionally excited) CO signal and the background CO signal on a pulse-to-pulse basis. This data acquisition mode is used only for $CO(v''=0)$; the method is unnecessary for the $CO(v''=1)$ measurements since no detectable background is observed. In the absence of background signal, it is verified that the same results are obtained with or without the subtraction mode.

The 6% mixture of H_2S in purified CO used in these experiments is made with Matheson CP grade (99.5%) H_2S and CO. The CO purification procedure[36,37] consists of slowly flowing CO first through a 1 m long Pyrex tube packed with copper filings and held in an oven at 400 °C, next through a 0.3 m LN_2 trap, and finally into an aluminum cylinder to a total pressure of 3 atm. The furnace is used to decompose iron and nickel carbonyl impurities, while the cold trap removes carbon dioxide and water. The purity as well as the relative H_2S and CO concentrations in the prepared mixture is verified using mass spectrometric analysis.

III. RESULTS

The total energy available from an H + CO collision is sufficient to excite CO to vibrational levels $v''\leqslant 5$. However, the relatively small T→V cross sections for producing the higher vibrational levels have limited our observations to only the $v''=0$ and $v''=1$ levels. The excitation spectra of the $A\,^1\Pi\leftarrow X\,^1\Sigma^+$ (0,0) and (1,1) vibrational bands are recorded with 15 pulses averaging and are shown in Fig. 1. The twofold advantage of choosing these particular vibrational bands is first, that they have large Franck–Condon factors,[38] and second, that the overlap of the (1,1) bandhead with the red wavelength edge of the (0,0) band provides a convenient means for relative intensity calibration. Excitation of the perpendicular electronic transition in CO gives rise to three (P, Q, and R) rotational branches. For our purposes, these P, Q, and R lines provide multiple measurements of the population in any given J'' level and thus serve as internal self-consistency checks in the extracted final state distributions.

A cursory scan of the (2,2) band has also been performed. The signal strength of the (2,2) bandhead is found to be ten times weaker than the (1,1) bandhead and thus is close to the lower limit of our detection sensitivity.

Rotational analyses of the observed spectra are carried out using the extensive data base of line frequencies and assignments of the CO Fourth Positive System.[39–41] The peak amplitudes are inverted to obtain populations using the relation

$$I(v'J'\leftarrow v''J'')\propto \nu\mu_{el}^2 S_{J'J''}q_{v'v''}N_{v''J''}/g_{J''}, \qquad (1)$$

where ν is the absorption frequency, μ_{el} the electronic transition moment, $S_{J'J''}$ the Hönl–London factor for the $\Pi\leftarrow\Sigma$ transition,[42] $q_{v'v''}$ the Franck–Condon factor, $g_{J''}$ the rotational degeneracy, and $N_{v''J''}$ the population of interest in the $(v''J'')$ level. Well-known perturbations of the A state $(v'J')$ levels can modulate the electronic transition moment by virtue of the v'- and J'-dependent variations in the $^1\Pi$ character of the excited state wave function. Tabulations[40,41] of the fractional $^1\Pi$ character as a function of $(v'J')$ level are used in order to invert correctly Eq. (1) to obtain $(v''J'')$ populations. It is to be understood that Eq. (1) is valid only when the following two conditions are met: (1) variations in fluorescence lifetimes of excited rotational–vibrational levels[43] are within the temporal gate width of the detection, and (2) the PMT spectral response to the total undispersed emission of excited levels is uniformly constant. Both criteria are satisfied in these experiments. Empirical proof of the second is obtained by recording a room temperature excitation spectrum of $CO(v''=0)$. The resulting rotational state distribution over the $0<J''<30$ range can be satisfactorily described by a linear Boltzmann plot with $T=298\pm 3$ K.

Figure 2(a) shows the CO rotational state distributions for the $v''=0$ and $v''=1$ levels, obtained from inverting the spectra of Fig. 1. When these data are plotted as the loga-

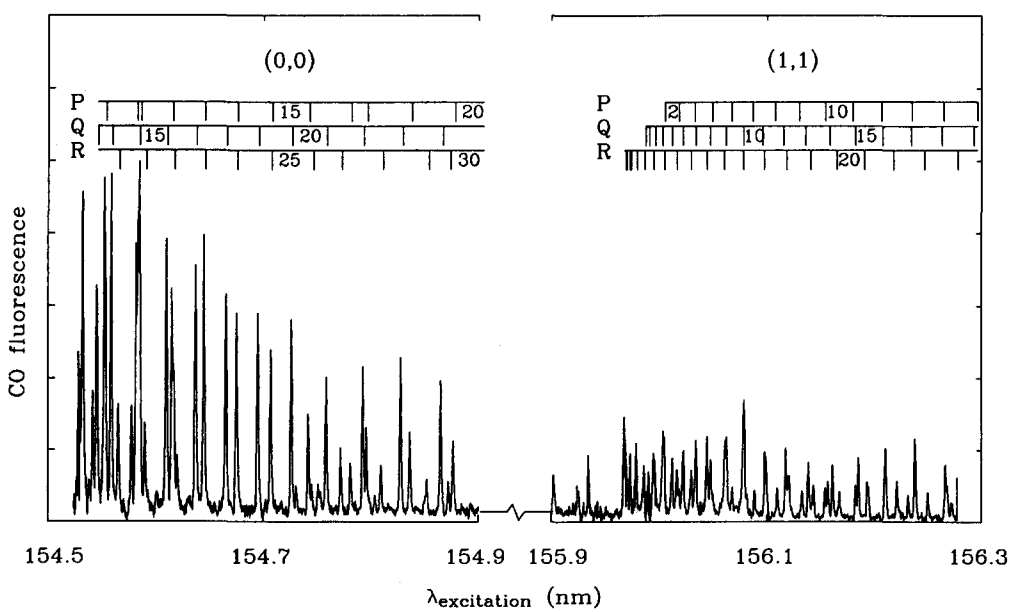

FIG. 1. Selected regions of the CO $A\,^1\Pi\leftarrow X\,^1\Sigma^+$ excitation spectra of the (0,0) and (1,1) bands. Frequency resolution is limited by the 0.6 cm^{-1} VUV laser linewidth.

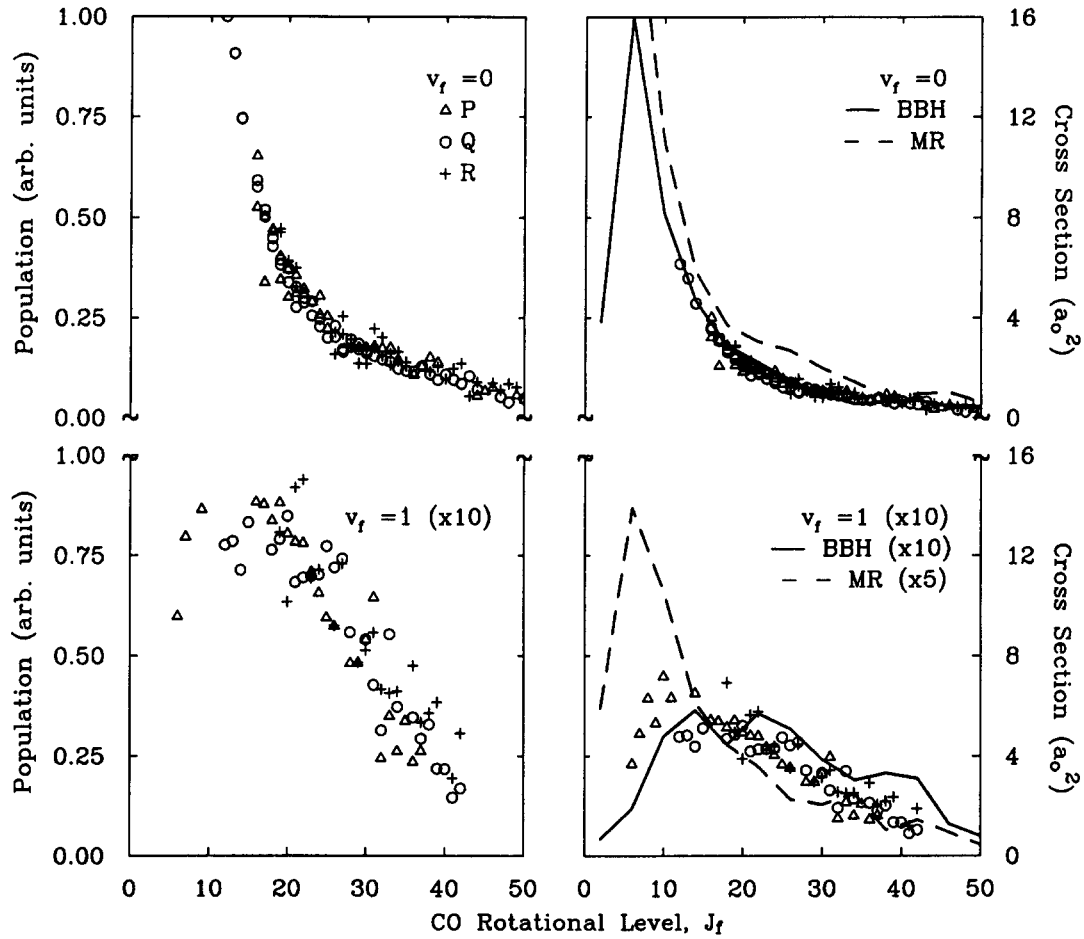

FIG. 2. (a) Observed rotational state distributions for the scattered CO in the $v''=0$ and $v''=1$ levels. (b) makes a comparison of the observed distributions with the QCT results. Any abrupt variation in the calculated distribution is a consequence of the rotational bin size of $\Delta J''=4$. Normalization of the cross sections is such that the sum over $J''=2$, 6, 10, 14,... equals the rotationally summed cross section $Q_{v''}$ in Table II. Note that the $v''=0$ MR cross section is not shown for $J''<8$ as it increases to a large value in that region. Also note that the $v''=1$ cross sections have been multiplied by ten on the BBH surface and by five on the MR surface for ease of display.

rithm of observed population vs rotational energy, one finds that the $v''=1$ data is apparently well described by a Boltzmann distribution with $T\simeq 1660$ K. By contrast, the $v''=0$ Boltzmann plot is notably bilinear; the $J''=12$–22 subset of data can be characterized with a $T\simeq 500$ K, whereas the remaining $J''>22$ data set has a $T\simeq 2880$ K. Using a $T\simeq 500$ K distribution for extrapolation to $J''=0$, we obtain an estimate of the rotationally summed vibrational populations. The population ratio of $CO(v''=1)/CO(v''=0)$ is found to be 0.1 ± 0.008, quoted to a 1σ statistical uncertainty.

The sensitivity of the experimental results to any possible $(H_2S)_n(CO)_m$ or pure CO clusters formed in the free jet expansion is now briefly addressed. Any substantial role played by $(H_2S)_n(CO)_m$ clusters can be ascertained by monitoring the temporal growth of collisionally excited $CO(v, J)$ product, starting from the initial preparation of fast H atoms with the H_2S photolysis laser pulse. We measure a linear dependence of the $CO(v, J)$ signal level over the $\Delta\tau=50$–400 ns range, which when extrapolated, yields a vanishing signal level for zero collision time. Therefore, we infer that the presence of any possible $(H_2S)_n(CO)_m$ clusters does not contribute to the principal results of the present work. It is also important to assess whether interferences from CO dimers or clusters significantly affect the H + CO collision results. In order to make this assessment, we have recorded the collisionally excited CO LIF spectra for two different stagnation pressures of the 6% H_2S + 94% CO premixture: 1 and 2 atm. Over this range of approximately four in cluster formation conditions, we measure essentially the same collisionally excited CO product state distribution. There are undoubtedly CO clusters present in the free jet expansion; however, jets of pure CO reportedly contain an insignificant fraction (5%) of CO dimers and even fewer of the larger aggregates.[44] Recently, Brechignac and coworkers[45] have found that optimal conditions favoring CO dimerization require seeded expansions of 10% CO dilution in He. Nearly pure samples of CO at 1–2 atm stagnation pressure do not apparently provide enough cooling for significant cluster formation. Since the $(H_2S)_n(CO)_m$ or pure CO clusters do not appear to cause measurable artifactual distortions of the present results, we attribute the recorded CO final state distributions to H + CO collision dynamics.

IV. DISCUSSION

A. Experimental product state distributions

As a point of reference, we can make a comparison of our observed CO rotational distributions with those expected from statistical considerations. The information–theoretic approach[46–48] to surprisal analysis is well suited for this purpose. Adopting a statistical prior is equivalent to stating that the probability of accessing any final state with energy E is proportional to the number of ways that the *remaining* energy $(E_{\text{total}}-E)$ can be distributed among the other translational and internal degrees of freedom of the system. Stated still more simply, a statistical distribution would arise

when all final states are equally probable irrespective of the initial conditions; the probability of ending up in any given (v'', J'') state is determined only by the degeneracy of the final level with quantum numbers (v'', J''). The *deviation* from such a statistical distribution provides a measure of the number of dynamical constraints governing a collisional event; this deviation is contained in the surprisal parameter I. The statistical or prior distribution $P^\circ(v, J)$, is given in the rigid rotor–harmonic oscillator[48,49] model by

$$P^\circ(g_r|f_v) \propto \tfrac{1}{2}(1-g_r)^{1/2}/(1-f_v). \quad (2)$$

Here, the reduced variables $f_v \equiv E_v/E_{\text{total}}$ and $g_r \equiv (E_r/E_{\text{total}})/(1-f_v)$ represent the fractional vibrational and rotational excitations, respectively. The rotational surprisal is defined as

$$I \equiv -\ln[P(g_r|f_v)/P^\circ(g_r|f_v)]. \quad (3)$$

For many reactions as well as inelastic scattering events,[50] the rotational surprisal is well represented by a linear function of the variable, g_r:

$$I(g_r) = \lambda_0 + \theta_r g_r, \quad (4)$$

where θ_r is the rotational surprisal parameter.

Figure 3 shows surprisal plots of our observed data. There is a stronger bias against rotational excitation of $v'' = 1$ as evidenced by the relatively larger value of $\theta_r = 8.5$ as compared to $v'' = 0$, where $\theta_r = 6.75$ for the high-J data. There is an additional point worth noting. The $v'' = 1$ data set can be uniformly well described by a linear surprisal plot. This one-parameter description implies that one dynamical constraint governs this combined vibrational–rotational excitation process. The predominantly bilinear plot for the $v'' = 0$ data implies that two dynamical constraints are in effect for these collision trajectories. The quasiclassical trajectory calculations of Sec. IV C reveal the identity of these constraints as essentially corresponding to the relative angle of approach of the H + CO collision partners.

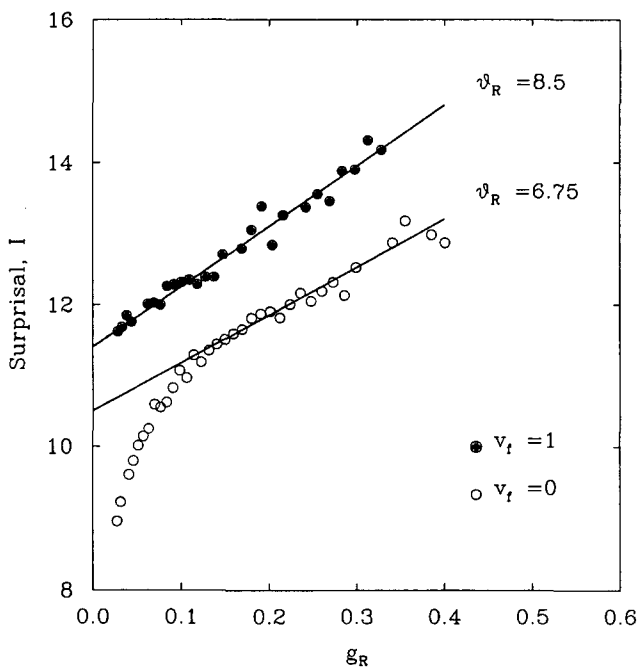

FIG. 3. Surprisal plots of the final rotational state distributions in CO $v'' = 0$ and $v'' = 1$ levels. Neither the observed nor the prior distributions have been normalized; therefore, the y intercept (i.e., λ_0) is not meaningful. The slope of the plot is, however, independent of the normalization; it yields a rotational surprisal parameter $\theta_r = 6.75$ for $v'' = 0$ and $\theta_r = 8.5$ for $v'' = 1$.

TABLE I. Comparison of BBH and MR surfaces.[a]

Species	Parameter	BBH	MR
HCO minimum	V relative to H + CO	−0.841	−0.809
	RCH	2.124	2.183
	RCO	2.259	2.224
	HCO angle	124.2	123
	harmonic frequencies	2749	2485
		1908	1865
		1157	1082
HCO saddle pt.	V relative to H + CO	0.069	0.069
	RCH	3.493	3.825
	RCO	2.180	2.173
	HCO angle	117.2	124
	harmonic frequencies	2121	1945
		399	405
		598*i*	611*i*
COH minimum	V relative to H + CO	0.841	1.041
	ROH	1.852	1.848
	RCO	2.455	2.434
	COH angle	111.7	114
	harmonic frequencies	3628	3162
		1387	1456
		1185	1046
COH saddle pt.	V relative to H + CO	1.457	1.503
	ROH	2.314	2.487
	RCO	2.262	2.353
	COH angle	119.2	141
	harmonic frequencies	2103	1117
		980	960
		3130*i*	1284*i*
Isomerization saddle pt.	V relative to H + CO	2.107	2.301
	RCH	2.493	2.512
	RCO	2.453	2.438
	ROH	2.165	2.154
	harmonic frequencies	2519	2956
		1464	228
		2305*i*	1645*i*

[a] All distances are in bohr, angles in degrees, frequencies in cm^{-1}, energies in eV.

B. Trajectory studies

To provide a quantitative comparison between theory and experiment, we have used the BBH and MR potential energy surfaces in a three-dimensional quasiclassical trajectory study of H + CO. Details of the calculations are very similar to those reported previously[21] except that the collision energy is here taken to be 1.58 eV, and no correction for multiple collision effects is used. 4000 trajectories were integrated on each potential surface, and the final state vibration/rotation quantum numbers were determined by rounding off the vibrational action and rotational angular momentum to the nearest multiple of $\hbar$. Following earlier calculations, the maximum impact parameter was taken to be 4.01 a_0 on the BBH surface[22] and 6.62 a_0 on the MR surface.[28]

Table I presents a comparison of the minima and saddle point properties of the BBH and MR surfaces. Since the MR

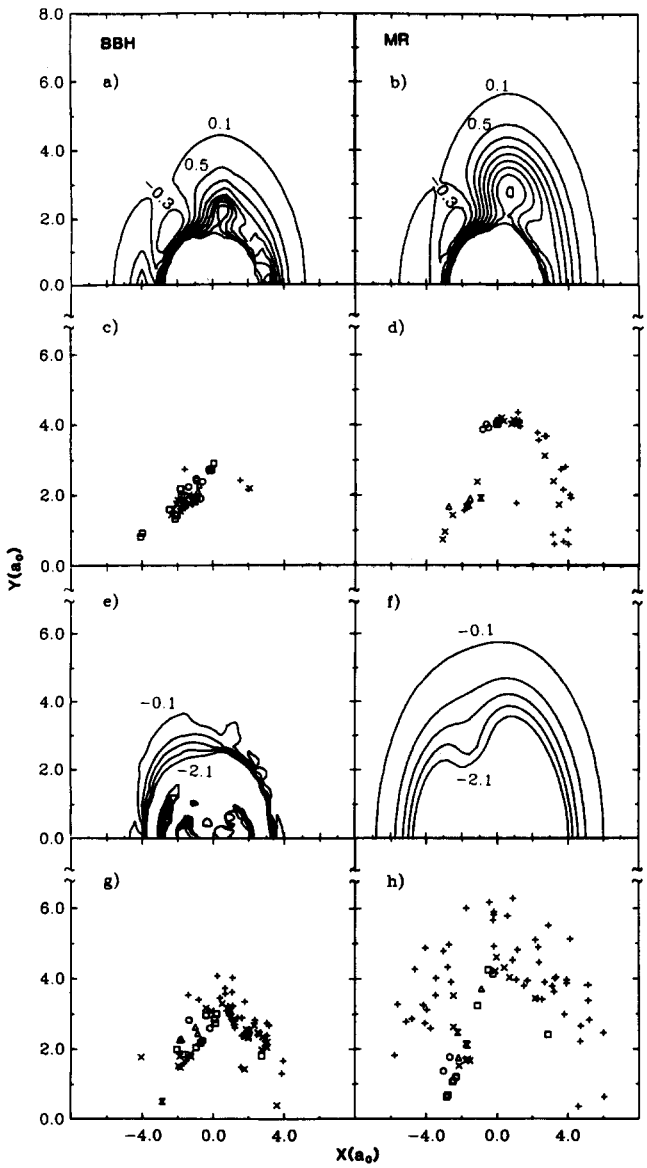

FIG. 4. (a) Contours of the BBH potential surface for a fixed CO distance of 2.173 a_0 (the equilibrium value for isolated CO). X and Y are the coordinates of the H atom relative to the center of mass of CO. The CO is taken to be along the X axis with C to the left of O. The energy is minimized with respect to the CO distance at each H atom location. Contours range in units of 0.4 eV starting at -0.3 eV, with zero taken to be H + CO at infinite separation. (b) Contours of the MR potential surface analogous to those in (a) and with the same choice of contours. The CO equilibrium distance in this case is 2.1322 a_0. (c) X and Y locations of the inner translational turning point locations for trajectories on the BBH surface producing CO with $v'' = 1$. Coordinates are taken from a random sample of 500 trajectories. The symbols used indicate rotational excitation as follows: $J'' = 0$–10(+), $J'' = 10$–20(×), $J'' = 20$–30 (square), $J'' = 30$–40 (circle), $J'' = 40$–50 (triangle), $J'' = 50$–60 (hour glass). (d) X and Y turning point coordinates as in (c) but for the MR surface. (e) Contours of the derivative of the BBH surface with respect to the CO internuclear distance. Contours range from -2.1 eV/a_0 in increments of 0.5 eV/a_0. Note that the large derivatives which occur near the origin [at $(X^2 + Y^2)^{1/2} < 3\ a_0$] are unimportant because they are at energetically inaccessible locations. (f) Contours of the derivative of the MR surface analogous to those in (e). (g) Inner turning points on the BBH and (h) on the MR surfaces for the $v'' = 0$ final state. Note that on both surfaces there is a sharp distinction between $J < 20$ and $J > 20$.

surface was developed so as to reproduce the BBH geometries and energies at these points, it is not surprising that they agree. The MR surface was also optimized to fit the known force constants for the HCO minimum and was partially optimized to fit the COH force constants. We note that the MR frequencies for these minima are in good agreement with BBH. The saddle point frequencies were not fit by MR, but the HCO saddle point frequencies are in good agreement with BBH. The COH and isomerization saddle point frequencies are sometimes quite different, however.

Figures 4(a) and 4(b) present contour plots of the BBH and MR potential surfaces as a function of the H atom location. For each plot, the CO distance has been fixed at its equilibrium value. Notice that although the two surfaces are qualitatively similar, there are some quantitative differences. The most notable difference is in the position of the maximum that occurs perpendicular to the CO bond outside the isomerization saddle point. This is farther out on the MR surface, and as a result, the MR surface is much longer ranged than BBH in this perpendicular direction.

C. Comparison with trajectory calculations

Figure 2(b) presents the rotational distributions for the BBH and MR surfaces for $v'' = 0$ and 1 as obtained from the trajectory calculations, and Table II summarizes the rotationally summed cross sections $Q_{v''}$, the probabilities $P_{v''}$, and the average J'' values $\langle J_{v''} \rangle$ for each surface. Included in Table II is a decomposition of the cross sections and $\langle J_{v''} \rangle$ values into contributions from collisions of H with the carbon end of CO (labeled with the superscript CH) and with the oxygen end of CO (labeled OH). This decomposition is based on which distance (CH or OH) has the smallest minimum value during each collision.

A comparison of the experimental data with the results of the trajectory calculations is presented in Fig. 2, where the observed distributions are scaled to be equal to the BBH distribution at $v'' = 0, J'' = 12$. The scaling is necessary because the experimental technique gives relative cross sections rather than absolute ones. Comparison of experiment with theory shows that the BBH relative rotational populations are in excellent quantitative agreement with experiment for both $v'' = 0$ and $v'' = 1$. The MR distributions are also in agreement for $v'' = 0$ but are noticeably different for $v'' = 1$, with the MR distribution peaking at a much lower

TABLE II. Comparison of product state distributions.[a]

v''	$Q_{v''}$	$P_{v''}$	$\langle J_{v''} \rangle$	$Q_{v''}^{CH}$	$\langle J_{v''} \rangle^{CH}$	$Q_{v''}^{OH}$	$\langle J_{v''} \rangle^{OH}$
BBH							
1	4.6	0.64	24	4.3	25	0.3	19
2	2.1	0.29	19	2.1	19	b	···
3	0.5	0.07	17	0.5	17	b	···
MR							
1	11.7	0.86	16	4.6	27	7.0	8
2	1.8	0.13	15	0.5	31	1.4	10
3	0.1	0.01	14	0.09	21	0.05	3

[a] All cross sections in a_0^2.

[b] Not statistically significant.

rotational state than experiment. The rotationally summed ratio of $v''=1$ to $v''=0$ cross sections on the BBH surface (0.11) is in much better agreement with experiment (0.1 ± 0.008) than is that obtained on the MR surface (0.31).

An examination of Table II indicates that the BBH cross section for $v''=1$ is 2.5 times smaller than the MR cross section, and that the MR vibrational distribution drops off more quickly with v'' than BBH. The difference between the amount of rotational excitation on BBH than on MR (as measured by $\langle J_{v''} \rangle$) is seen to persist to higher v'', although the actual values of $\langle J_{v''} \rangle$ decrease with increasing v'' on both surfaces.

The origin of the difference between the BBH and MR rotational distributions for $v''=1$ is apparent from the partial cross sections $Q_{v''}^{CH}$ and $Q_{v''}^{OH}$ in Table II. Here we find that only $Q_{v''}^{CH}$ is large on the BBH surface while both $Q_{v''}^{CH}$ and $Q_{v''}^{OH}$ are large on MR. If we consider collisions of H with the carbon atom of CO, then the BBH and MR values of Q^{CH} and $\langle J_{v''} \rangle^{OH}$ are almost the same. However, the $Q_{v''}^{OH}$ values are quite different, and since the $\langle J_{v''} \rangle^{CH}$ value for MR is small, the overall rotational distribution is colder on MR.

To further assess the differences between BBH and MR, in Figs. 4(c) and 4(d) we plot the locations of the inner turning points associated with a random ensemble of trajectories at 1.58 eV that all give $v''=1$ as the final state. Figure 3(c) which shows the BBH results is exactly as expected from Table II in that almost all the inner turning points are located on the carbon side of CO, and most of these are on the inner repulsive wall of the HCO well. Figure 4(d), which shows the MR results, indicates that collisions with the oxygen atom end of CO are of major importance. Many of the collisions are associated with exterior regions of the potential that are well removed from even the COH well, and nearly all of them are associated with low rotational excitation.

Figures 4(e) and 4(f) plot contours of the derivatives of the BBH and MR potential surfaces with respect to the CO distance. To a first approximation, vibrational excitation occurs when trajectories penetrate to regions of the potential surfaces where the magnitude of this derivative is large, i.e., to regions where the force on the CO coordinate is high. By comparing Figs. 4(a) and 4(e), one sees that such penetration can occur on the BBH surface easily only in the HCO well region. On the O atom side of the CO, the derivative becomes large only at points where the energy is >1.58 eV above the asymptote. Consequently, CO is excited to $v''=1$ mainly in collisions that sample the HCO well. On the MR surface, Figs. 4(b) and 4(f) show that penetration to regions of large derivative can occur for almost all directions of H atom approach. In fact, the -0.1 eV/a_0 derivative contour in Fig. 4(f) is always outside the 0.1 eV contour in Fig. 4(b). Thus, it is not surprising that $v''=1$ is produced in collisions that strike the molecule in any orientation.

We can address the energy transfer mechanism governing pure rotational excitation of the CO($v''=0$) product in a manner similar to that used above for the CO($v''=1, J''$) product. Figures 4(g) and 4(h), respectively, illustrate the calculated turning points of the rotationally inelastic but vibrationally elastic collisions on the BBH and MR potential surfaces. For both surfaces, turning points for low J'' excitation of CO are found to be generally delocalized in space, whereas high J'' excitation occurs over a more restricted range of H···CO approach angles, centered near the bond angle of the stable HCO radical. The interpretation is fairly straightforward: high rotational excitation results primarily from collisions for which the H atom penetrates into the steep, inner repulsive wall of the HCO potential well. A smaller extent of rotational excitation takes place at all other approach angles outside the HCO well, where strong repulsive interaction between collision partners does not dominate.

These QCT results are consistent with the surprisal analysis of Sec. IV A. The relatively large value of the rotational surprisal parameter θ_r, describing the $v''=0$, $J''=12$–20 subset of data indicates that these data strongly deviate from a statistical prior distribution. In other words, the production of low-J'' excitation comes from short-lived collisions of a purely direct and impulsive nature. By contrast, the smaller value of θ_r describing the $v''=0$, $J''>20$ subset of data implies that collisions producing these levels are of a more long-lived nature. Consequently, the resulting $J''>20$ distribution begins to more closely resemble a statistical distribution, for which $\theta_r=0$. Our inference is that the high-J'' promoting collisions are more likely to proceed through a collision-complex, albeit a short-lived one.

Overall, we find that there is a significant difference between the BBH and MR results and that the comparison with experiment indicates the BBH surface to be more accurate. The origin of the difference between the two surfaces has been traced to the outer repulsive part of the oxygen side of the H + CO interaction potential. The reason why collisions with this region of the potential give no vibrational excitation on BBH but substantial excitation on MR is that the MR surface has a large CO stretch derivative at locations that are easily sampled by the trajectories, while the BBH surface does not.

V. CONCLUSIONS

The measured CO vibrational and rotational state distributions resulting from 1.58 eV H + CO collisions are found to be in very good agreement with results of quasiclassical trajectory calculations performed on the BBH potential surface. A detailed examination of the trajectories revealed the primary mechanism for optimal vibrational energy transfer in this system; the hydrogen atom must approach the carbon end of carbon monoxide with an H···CO angle of $\simeq 50°$–$60°$. Since this range of angles also corresponds to a large moment arm for exerting a torque on the CO ellipsoid, vibrational excitation of CO is necessarily accompanied by substantial rotational excitation.

The two H + CO potential surfaces discussed in this work differ dramatically in their ability to promote CO vibrational excitation. The MR potential surface allows substantial vibrational energy transfer as a result of end-on and/or broadside collisions. Adjustments of the COH-complex regions of the MR surface (which incorrectly predict the extent of rotational–vibrational energy transfer) are

especially necessary since similar portions of this MR surface are used for the interpretation of $H + CO_2$ collision dynamics.[51]

The rotational distribution of $CO(v'' = 1)$ appears to be quite sensitive to the differences between the BBH and MR surfaces. While it is encouraging that these experiments are sensitive to the details of the surface, the results presented here indicate that it is probable that rather sophisticated surfaces will be needed to correctly predict the results of vibrational and rotational energy transfer, particularly when attractive forces are important.

Further experimental efforts are being directed towards the determination of angular distributions of the scattered CO product from H + CO collisions. Coarse estimates of the differential scattering cross sections can be made by coexpanding the reactants, as in this work, and recording the Doppler profiles of individual rotational lines of $CO(v'', J'')$. Since the precollision H atom angular distribution is well known, the CO Doppler profiles can be readily deconvoluted to yield the final, state-specific, CO angular distributions. In favorable cases, the possibility of extracting information on $(\mathbf{v},\mathbf{J})$ vector correlation of the CO product also exists.

While this work has involved 1.58 eV H + CO collisions, it would be useful to perform experiments at other collision energies in order to obtain a more extensive understanding of the collision dynamics. Experiments at a collision energy of 2.3 eV are currently underway.

ACKNOWLEDGMENTS

The authors express their appreciation to Dr. A. Sinha for alerting them to the necessity of purifying CO samples. We gratefully acknowledge Professor R. W. Field for providing volumes of data on CO perturbations. We also thank Dr. N. Sivakumar for preliminary work. Work at Cornell is supported by the Air Force Office of Scientific Research under Grant No. AFOSR-86-0017. G.C.S. wishes to acknowledge financial support from NSF Grant No. CHE-8416026 and helpful conversations with L. B. Harding, T. H. Dunning, and A. F. Wagner.

[1]G. W. Flynn and R. E. Weston, Jr., Annu. Rev. Phys. Chem. **37**, 551 (1986).
[2]C. R. Quick, R. E. Weston, Jr., and G. W. Flynn, Chem. Phys. Lett. **83**, 15 (1981).
[3]F. Magnotta, D. J. Nesbitt, and S. R. Leone, Chem. Phys. Lett. **83**, 21 (1981).
[4]C. A. Wight, F. Magnotta, and S. R. Leone, J. Chem. Phys. **81**, 3951 (1984).
[5]S. Datta, R. E. Weston, Jr., and G. W. Flynn, J. Chem. Phys. **80**, 4071 (1984).
[6]C. F. Wood, G. W. Flynn, and R. E. Weston, Jr., J. Chem. Phys. **77**, 4776 (1982).
[7]C. A. Wight and S. R. Leone, J. Chem. Phys. **78**, 4875 (1983).
[8]C. A. Wight and S. R. Leone, J. Chem. Phys. **79**, 4823 (1983).
[9]J. O. Chu, G. W. Flynn, and R. E. Weston, Jr., J. Chem. Phys. **78**, 2990 (1983).
[10]J. O. Chu, C. F. Wood, G. W. Flynn, and R. E. Weston, Jr., J. Chem. Phys. **80**, 1703 (1984).
[11]J. O. Chu, C. F. Wood, G. W. Flynn, and R. E. Weston, Jr., J. Chem. Phys. **81**, 5533 (1984).
[12]J. A. O'Neill, J. Y. Cai, G. W. Flynn, and R. E. Weston, Jr., J. Chem. Phys. **84**, 50 (1986).
[13]J. A. O'Neill, J. Y. Cai, C. X. Wang, G. W. Flynn, and R. E. Weston, Jr. (in press).
[14]S. A. Hewitt, J. F. Herschberger, G. W. Flynn, and R. E. Weston, Jr., J. Chem. Phys. **87**, 1894 (1987).
[15]C. R. Quick, Jr., and D. S. Moore, J. Chem. Phys. **79**, 759 (1983).
[16]C. A. Wight, D. J. Donaldson, and S. R. Leone, J. Chem. Phys. **83**, 660 (1985).
[17]J. M. Bowman, J. S. Bittman, and L. B. Harding, J. Chem. Phys. **85**, 911 (1986).
[18]H. Y. Wang, J. A. Eyre, and L. M. Dorfman, J. Chem. Phys. **59**, 5199 (1973).
[19]K. K. Murray, T. M. Miller, D. G. Leopold, and W. C. Lineberger, J. Chem. Phys. **84**, 2520 (1986).
[20]M. -C. Chuang, M. F. Foltz, and C. B. Moore, J. Chem. Phys. **87**, 3855 (1987); C. K. Moortgat, W. Seiler, and P. Warneck, *ibid.* **78**, 1185 (1983).
[21]L. C. Geiger and G. C. Schatz, J. Phys. Chem. **88**, 214 (1984).
[22]L. C. Geiger, G. C. Schatz, and L. B. Harding, Chem. Phys. Lett. **114**, 520 (1985).
[23]T. H. Dunning, J. Chem. Phys. **73**, 2304 (1980).
[24]K. S. Sorbie and J. N. Murrell, Mol. Phys. **29**, 1387 (1975).
[25]L. C. Geiger, G. C. Schatz, and B. C. Garrett, in *Resonances in Electron–Molecule Scattering, van der Waals Complexes, and Reactive Chemical Dynamics*, edited by D. G. Truhlar (American Chemical Society, Washington, D. C., 1984), Chap. 22.
[26]H. Romanowski, K. -T. Lee, J. M. Bowman, and L. B. Harding, J. Chem. Phys. **84**, 4888 (1986).
[27]K. -T. Lee and J. M. Bowman, J. Chem. Phys. **85**, 6225 (1986); **86**, 215 (1987).
[28]J. N. Murrell and J. A. Rodriguez (preprint).
[29]G. N. A. Van Veen, K. A. Mohamed, T. Baller, and A. E. DeVries, Chem. Phys. **74**, 261 (1983).
[30]The Newport BV-100 valve used here is patterned after the original design of T. E. Adams, B. H. Rockney, J. S. Morrison, and E. R. Grant, Rev. Sci. Instrum. **52**, 1649 (1981).
[31]L. C. Lee, X. Wang, and M. Suto, J. Chem. Phys. **86**, 4353 (1987).
[32]R. T. Hodgson, P. P. Sorokin, and J. J. Wynne, Phys. Rev. Lett. **32**, 343 (1974).
[33]S. C. Wallace and G. Zdasiuk, Appl. Phys. Lett. **28**, 449 (1976).
[34]P. P. Herman, P. E. La Rocque, R. H. Lipson, W. Jamroz, and B. P. Stoicheff, Can. J. Phys. **63**, 1581 (1985).
[35]I. Burak, J. W. Hepburn, N. Sivakumar, G. E. Hall, G. K. Chawla, and P. L. Houston, J. Chem. Phys. **86**, 1258 (1987).
[36]G. Karl, P. Kruus, and J. C. Polanyi, J. Chem. Phys. **46**, 224 (1967).
[37]W. Braker and A. L. Mossman, *Mathes on Data Handbook* (Matheson, New Jersey, 1980).
[38]P. H. Krupenie, Natl. Bur. Stand. (1966).
[39]R. W. Field, B. G. Wicke, J. D. Simmons, and S. G. Tilford, J. Mol. Spectrosc. **44**, 383 (1972).
[40]A. C. Le Floch, F. Launay, J. Rostas, R. W. Field, C. M. Brown, and K. Yoshino, J. Mol. Spectrosc. **121**, 337 (1987).
[41]R. W. Field (unpublished results).
[42]J. T. Hougen, Nat. Bur. Stand. Monogr. 115 (1970).
[43]M. Maeda and B. P. Stoicheff, in *Laser Techniques in the Extreme Ultraviolet*, edited by S. E. Harris and T. B. Lucatorto (AIP, New York, 1984), p. 162.
[44]D. Bassi, A. Boschetti, S. Marchetti, G. Scoles, and M. Zen, J. Chem. Phys. **74**, 2221 (1981).
[45]C. Chidiac, J. P. Martin, M. Y. Perrin, and Ph. Brechignac (private communication).
[46]R. D. Levine and R. B. Bernstein, Acc. Chem. Res. **7**, 393 (1974).
[47]R. D. Levine and J. L. Kinsey, in *Atom–Molecule Collision Theory*, edited by R. B. Bernstein (Plenum, New York, 1979), p. 693.
[48]R. B. Bernstein, *Chemical Dynamics via Molecular Beam and Laser Techniques* (Clarendon, Oxford, 1982), p. 196.
[49]J. L. Kinsey, J. Chem. Phys. **54**, 1206 (1971).
[50]D. P. Gerrity and J. J. Valentini, J. Chem. Phys. **83**, 2207 (1985).
[51]G. C. Schatz and M. S. Fitzcharles, Discuss. Faraday Soc. (to be published).